RSC Medicinal Chemistry

ROYAL SOCIETY OF CHEMISTRY

RESEARCH ARTICLE

View Article Online
View Journal | View Issue

Cite this: *RSC Med. Chem.*, 2025, **16**, 3567

Rational design of indolyl acrylamides as antibacterial agents targeting multidrug-resistant *Acinetobacter baumannii* strains†

Velvett G. Domínguez-Méndez, [a] Rosa María Chávez-Santos, [a] Karol Carrillo-Jaimes, [b] Alejandra Hernández-Santoyo, [c] Santos Ramírez-Carreto, [c] Armando Hernandez-Garcia, [c] Rodrigo Aguayo-Ortiz, [d] Corina-Diana Ceapă, [b] José Rivera-Chavéz [b] and Roberto Martínez *[a]

Antimicrobial resistance (AMR) has become a significant public health problem. This study investigated the structure–activity relationship of indole core molecules to uncover novel antimicrobials against resistant bacteria. Their antimicrobial evaluation against ESKAPEE bacteria showed superior efficacy compared to cefepime, meropenem, ciprofloxacin, and gentamicin against multidrug-resistant *A. baumannii* strain A-564, with minimum inhibitory concentration (MIC) values of 4.3 and 1.2 μg mL^{-1} for compounds **12e** and **12j**, respectively. Also, the same compounds showed better activity than cefepime for *A. baumannii* BAA ATCC 747 with MIC values of 1.2 and 4.4 μg mL^{-1}. In addition, **12e** and **12f** showed activity against methicillin- and penicillin-resistant *S. aureus* with MIC values of 3.2 and 2.1 μg mL^{-1}. Furthermore, the highly active compounds **12e** and **12j** exhibited low toxicity, with hemolysis values >40 μg mL^{-1}. Preliminary examination of the mechanism of action revealed that **12e** could exhibit dose-dependent inhibition of the *Ab*FtsZ$_{1-412}$ enzyme from strain XDR A-564, achieving 51% inhibition of GTPase activity at 32 μg mL^{-1}, thus altering the binary fission process, which could be attributed to the fact that **12e** binds to the GTP site and interferes with the function of the enzyme by inhibiting the formation of the Z-ring. Also, a cell viability assay indicates that cells treated with these compounds showed increased permeability, compromising the stability of the *A. baumannii* A-564 membrane. These results provided valuable information for further developing indolyl-acrylamides as new antimicrobial agents.

Received 14th February 2025,
Accepted 12th May 2025

DOI: 10.1039/d5md00145e

rsc.li/medchem

1. Introduction

Antimicrobial resistance (AMR) represents a significant global threat to public health.[1] In 2019, AMR was associated with approximately 4.95 million deaths.[2] The World Health Organization (WHO) projects that AMR could result in up to 10 million deaths per year by 2050.[3] Clinically significant multidrug-resistant pathogens group under the ESKAPEE acronym, which includes: *Enterococcus faecium*, *Staphylococcus aureus*, *Klebsiella pneumoniae*, *Acinetobacter baumannii*, *Pseudomonas aeruginosa*, *Enterobacter* spp., and *Escherichia coli*.[4] These bacteria, prevalent in hospital settings, have developed multidrug resistance (MDR), extreme drug resistance (XDR) or pandrug resistance (PDR) making them particularly dangerous.[5] The WHO recently updated its list of priority pathogens for antibiotic research and development, placing carbapenem-resistant *A. baumannii* among the top three bacteria in group one, classified as a critical priority.[6] Clinical isolates of this bacterium, such as the extensively drug-resistant (XDR) strain A-564 from a Mexican patient, have shown resistance to various drug families, including quinolones, aminoglycosides, penicillins, cephalosporins, carbapenems, and macrolides.[7] Hence, developing new and effective antibacterial drugs to address MDR and XDR strains is crucial.

Designing bioactive molecules and conducting structure–function studies offer targeted and efficient approaches to

[a] *Departamento de Química Orgánica, Instituto de Química, Universidad Nacional Autónoma de México, Circuito Exterior, Ciudad Universitaria, Alcaldía Coyoacán, C.P. 04510, Cd de Mx, Mexico. E-mail: robmar@unam.mx*
[b] *Laboratorio of Microbiología, Departamento de Productos Naturales, Instituto de Química, Universidad Nacional Autónoma de México, Circuito Exterior, Ciudad Universitaria, Alcaldía Coyoacán, C.P. 04510, Cd de Mx, Mexico*
[c] *Departamento de Química de Biomacromoléculas, Instituto de Química, Universidad Nacional Autónoma de México, Circuito Exterior, Ciudad Universitaria, Alcaldía Coyoacán, C.P. 04510, Cd de Mx, Mexico*
[d] *Departamento de Farmacia, Facultad de Química, Universidad Nacional Autónoma de México, Circuito Exterior, Ciudad Universitaria, Alcaldía Coyoacán, C.P. 04510, Cd de Mx, Mexico*

† Electronic supplementary information (ESI) available. See DOI: https://doi.org/10.1039/d5md00145e

drug discovery, reducing the time and resources required compared to the extensive testing of large chemical libraries. One of such alternative drug discovery approaches is searching for privileged structures – molecular frameworks that confer biological activities in diverse pharmacological targets.[8] This approach has shown promising results in finding pharmacologically active compounds across a broad range of therapeutic areas. Several reviews on the topic of privileged structures[8] support the idea that the indole ring is one of the best-known privileged structures and exerts various pharmacological activities depending on the functional groups joined to the moiety.[9] Examples of bioactive compounds bearing the indole scaffold are panobinostat (**1**) for the treatment of multiple myeloma,[10] ramosetron (**2**) as an antiemetic and as a treatment for irritable bowel syndrome,[11] sumatriptan (**3**) for the treatment of migraine,[12] and aterviridine (**4**) with activity against human immunodeficiency virus (HIV-1)[13] (Fig. 1).

Moreover, the indole-containing scaffold is a key structural feature in many compounds that inhibit the growth of Gram-negative and Gram-positive bacteria.[10] The synthesis of a series of 3-amino indoles was previously reported, and their antibacterial properties were evaluated against ESKAPEE group bacteria. Among these, compound **5** (Fig. 1) demonstrated significant inhibitory activity against ciprofloxacin-resistant *A. baumannii* and *P. aeruginosa* with a MIC of 8 μg mL^{-1} for both strains.[14] Compound **6** (Fig. 1) demonstrated an even more potent activity against MDR and XDR strains, especially when combined with carbapenems. It also exhibited broad-spectrum efficacy against Enterobacteriaceae, with an MIC_{90} value of 1–2 μg mL^{-1}. The study suggested that incorporating a primary amine into molecules that meet specific structural and rigidity requirements enhances accumulation in bacterial cells, thereby boosting antibacterial potency.[15,16] Compound **7** (Fig. 1) showed promising activity with MIC values ranging from 1 μg mL^{-1} to 4.8 μg mL^{-1} against several drug-sensitive bacteria, including *S. aureus* ATCC 25923, *S. aureus* ATCC 26003, *E. faecalis* ATCC 29212, *B. subtilis* ATCC 63501, and *E. coli* ATCC 44568. Additionally, this antimicrobial agent exhibited activity against both Gram-positive and Gram-negative MDR bacteria, specifically *E. coli* BAA-196 and *S. aureus* ATCC 43300 (MRSA), with MIC values as low as 0.5 μg mL^{-1} for both strains.[17] Interestingly, in the same year that compound 7 was reported, Yuan, W. *et al.*[18] discovered a very similar indole derivative (compound **8**), (Fig. 1) which presented excellent activity against *S. aureus* ATCC 29247 (ampicillin-resistant), *E. faecalis* 51575, and *E. faecium* 700221, both vancomycin-resistant, with MIC values between 2 and 4 μg mL^{-1}. Upon investigating the antibacterial mechanism of compound **8**, it was found that, at a concentration of 8 μg mL^{-1}, this molecule inhibits 60% of the GTPase activity of the *Sa*FtsZ enzyme. This closely aligns with previous observations of other indole derivatives, where bacterial growth inhibition was linked to the disruption of FtsZ activity.[19] FtsZ is a temperature-

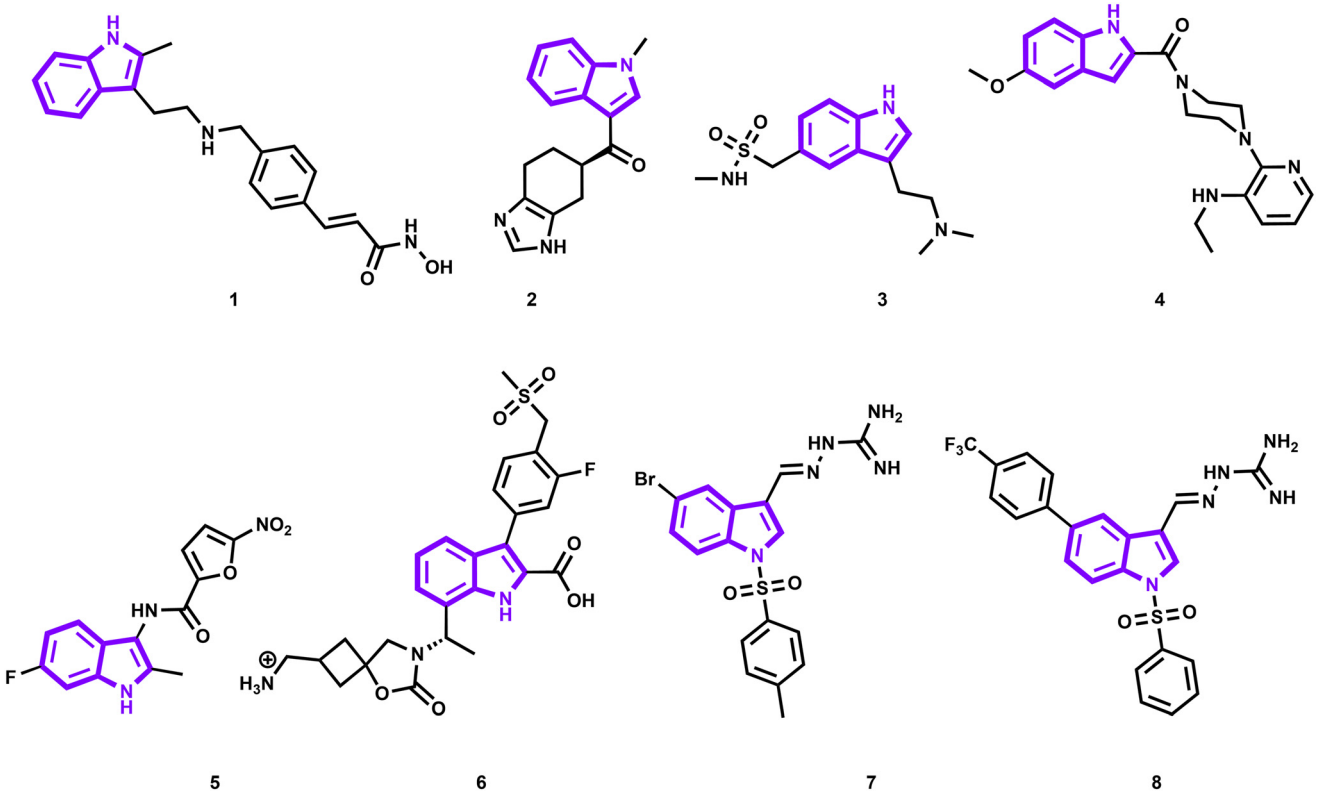

Fig. 1 Examples of compounds containing indole scaffolds and exhibiting biological activity.

sensitive filamentous protein involved in bacterial cell division that assembles into a circumferential structure known as the Z-ring.[20] This process requires guanosine-5′-triphosphate (GTP) binding and hydrolysis (GTPase activity), along with stabilization and anchoring of FtsZ to cytoplasmic membrane-binding proteins. Once the Z-ring is formed, it recruits a series of additional proteins necessary for cytokinesis.[21] To date, only a limited number of antimicrobial agents have been identified that bind to this protein and modulate its polymerization or GTPase activity.[22] Nevertheless, as the FtsZ protein is highly conserved and essential across bacterial species, it represents a promising yet underexplored target for the development of new antimicrobial agents.[22]

This research centers on the design and synthesis of indole-based compounds, inspired by the remarkable antibacterial activity and mechanisms of action of compounds **7** and **8** (Fig. 1). By conducting a comprehensive structure–activity relationship (SAR) study, we aim to delve into their antimicrobial properties and elucidate potential modes of action, also showing that the strategic design of bioactive molecules and the application of structure–function studies provide a focused and efficient pathway for drug discovery, significantly cutting down on the time and

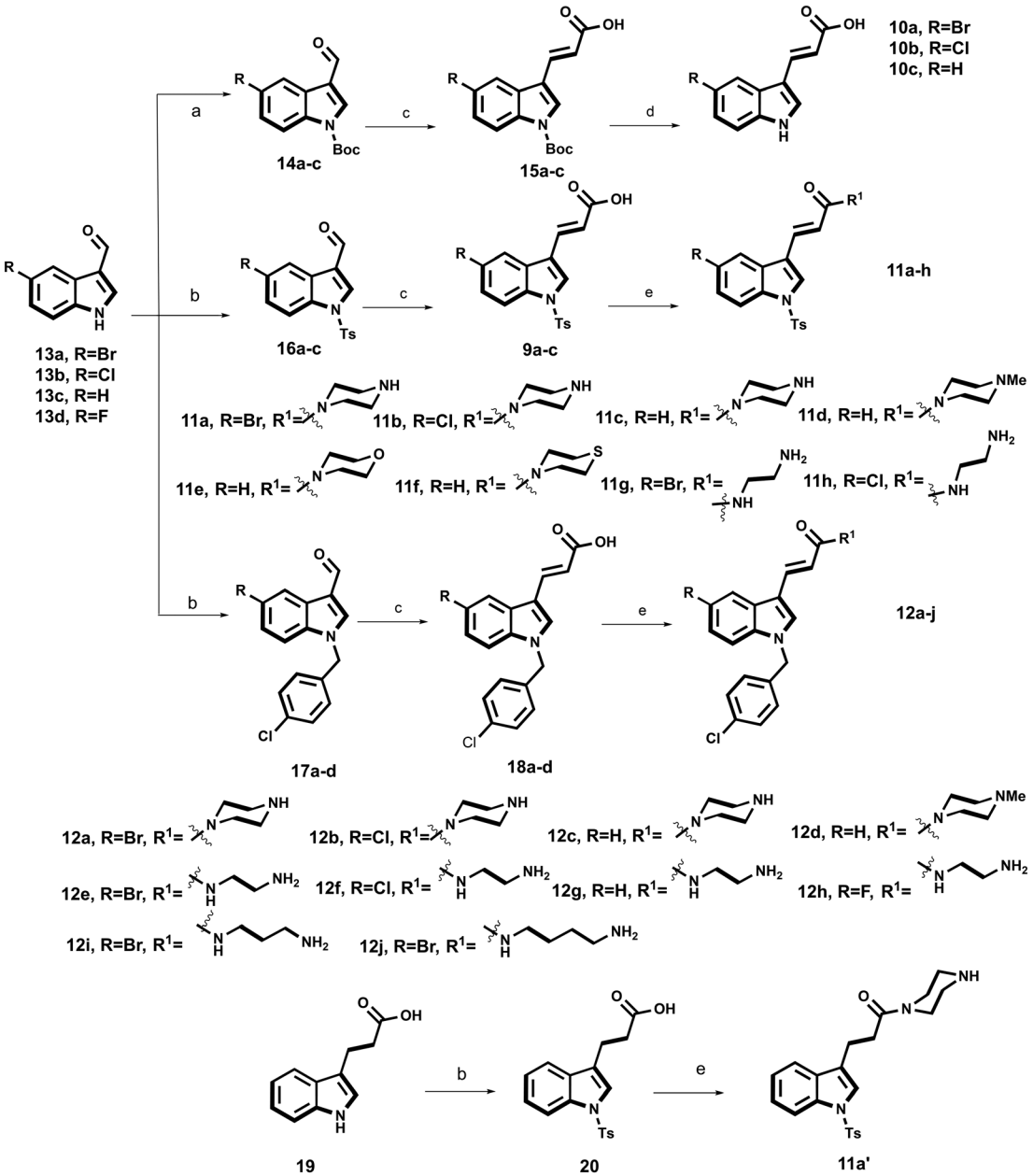

Scheme 1 Synthetic route for the indolyl acrylamides analogues **11a**–**h**, **11a**′ and **12a**–**j**. a) **13a**–**c**, Boc_2O, NaH, THF, rt, 24 h; b) **13a**–**c**, *p*-toluenesulfonyl chloride or *p*-chlorobenzyl chloride, NaOH, and TEBAC, DCM, rt, 16 h; c) **14a**–**c** or **16a**–**c**, **17a**–**c**, malonic acid, piperidine, pyridine, 80 °C, 5 h; d) **15a**–**c**, TFA, DCM, rt, 1 h; e) **9a**–**c** or **18a**–**d**, HBTU, DIPEA, DCM/DMF (3 : 1), rt, 5 h.

resources needed compared to the broad testing of large chemical libraries. Our goal is to contribute to significant advancements in antimicrobial research, paving the way for the development of novel and effective antibacterial agents.

2. Results and discussion

2.1 Chemistry

Compounds **9a–c**, **10a–c**, **11a–h**, **11a′**, and **12a–j** were synthesized through the efficient routes outlined in Scheme 1, demonstrating the effectiveness and productivity of our process. Initially, compounds **15a–c**, **9a–c**, and **18a–d** were synthesized in two steps, with the first step involving the indole N–H substitution of compounds **13a–c** with Boc, Ts, and *p*-Cl-benzyl groups. *N*-substitution with Boc was carried out using Boc_2O and NaH in THF at rt for 24 h obtaining the *N*-Boc compounds **14a–c** in 89–96% yields.[23] The *N*-Ts intermediates **16a–c** were obtained by stirring **13a–c** with *p*-toluene sulfonyl chloride, NaOH, and catalytic amounts of benzyltriethylammonium chloride (TEBAC) in DCM at rt for 16 h, in 81–94% yields.[24] Similarly, compounds **17a–d** were prepared using **13a–d**, *p*-chlorobenzyl chloride, NaOH and TEBAC. The second step was a Knoevenagel condensation reaction of **14c**, **16a–c** and **17a–d** with malonic acid, *via* the Doebner modification to obtain **15a–c**, **9a–c**, and **18a–d** in 84–93% yields.[25]

Conversely, compounds **10a–c** were obtained by acid hydrolysis of **15a–c** with trifluoroacetic acid (TFA) in DCM, with yields between 68 and 78%.[26] Likewise, the coupling of indolylacrylic acids **9a–c** or **18a** and the corresponding amine was achieved using HBTU and DIPEA in DCM/DMF (1 : 3 v/v), giving compounds **11a–h** and **12a–j** in 13–68% yields.[27] Finally, compound **11a′** was prepared by stirring **19** with *p*-toluene sulfonyl chloride in DMC at rt for 24 h, followed by a coupling reaction with HBTU, DIPEA, and piperazine in DCM/DMF (1 : 3 v/v) at rt for 5 h, obtaining compound **11a′** with a 43% yield.[27] The structures of all compounds were confirmed by ^{1}H and ^{13}C NMR spectroscopy and high-resolution mass spectrometry (ESI-HRMS). For example, in the ^{1}H NMR spectrum of compound **12e**, the signals for the 2-*N*-amino-ethyl group are evident, including one triplet at approximately 2.70 ppm for C-2′ and one quartet at 3.22 ppm for C-1′. Two doublets were also observed at 6.58 and 7.51 ppm, corresponding to the unsaturated α–β system, with a J = 15.9 Hz indicating the *trans* conformation of the alkene. Moreover, the *AA′BB′* system for the aromatic ring of the *p*-Cl-benzyl substituent was also observed.

Additionally, we observed in the ^{13}C NMR spectrum of **12e** a peak at 166.18 ppm corresponding to the carbonyl group of the α–β unsaturated amide, as well as the carbons for the ethylenediamine motif at 41.09 and 41.42 ppm and the methylene at 48.65 ppm of the *p*-Cl-benzyl group. When the compound is **12j**, the signals for the 2-*N*-amino-butyl group are a triplet at 2.99 ppm, with another at 3.36 ppm corresponding to C-1′ and C-4′, and a multiplet at 1.69–1.71 ppm corresponding to the two central methylene's CH_2–2′ and CH_2–3′. Also, the structure of the synthesized compound **12j**, with a molecular formula $C_{22}H_{24}BrClN_3O$, was supported by the HRMS spectrum, where the molecular ion peak ESI^+ m/z 460.07892 $(M + H)^+$ is in concurrence with the calculated value of 460.07913. Similarly, the ESI-HRMS results were consistent with all the synthesized structures.

2.2 Antibacterial studies

Compounds **9a–c**, **10a–c**, **11a–j**, **11a′**, and **12a–j** were screened against a panel of bacterial strains, including *Acinetobacter baumannii* ATCC BAA 747 and ATCC 17978, as well as the extensively drug-resistant (XDR) clinical strain of Mexican origin A-564, and against other bacteria of the ESKAPEE group: *S. aureus* (MRSA), *S. aureus* ATCC 25923, *K. pneumoniae* K2 (MDR), and *P. aeruginosa* P-48M (MDR). We used cefepime, gentamicin or colistin as controls (Table 1). MIC values were determined using a plate microdilution assay following the guidelines of the Clinical and Laboratory Standards Institute (CLSI).[28] Percentages were afterwards calculated using GraphPad Prism 9.5.1.

2.3 Structure–activity relationship discussion

We started with structural simplification to evaluate the antimicrobial structure–function relationship. The exchange of a basic group (guanidinium) for an acidic group was explored, resulting in compounds **9a–c** (Fig. 2), evaluated at an initial concentration of 50 μg mL^{-1}. Compounds **9a** (C5–Br) and **9b** (C5–Cl) showed 72% to 100% inhibition against *A. baumannii* BAA ATCC 747. Compound **9a** stood out by achieving 39% inhibition against *A. baumannii* XDR strain A-564. Attempting to further simplify the structure, the tosyl indole group was replaced by a hydrogen, which resulted in a considerable decrease in potency of the resulting **10a–c** molecules against all tested *A. baumannii* isolates (see ESI† Table S1, page S16), indicating the importance of the indole *N*-sulfonamide group for the antibacterial activity.[29] These findings prompted the hypothesis that systematic exploration of structural modifications to the compounds could enhance their bioactivity. Compounds **9a–c** were selected as hit molecules for further optimization (Fig. 2). Since piperazine-derived compounds have been previously reported as antibacterial agents, we replaced the carboxylic acid in the core structure with a piperazinyl group, thus obtaining **11a–c** (Table 1).[30] Compounds **11a–c**, as well as the compounds resulting from the subsequent structural modifications, were evaluated against *A. baumannii* BAA ATCC 747, ATCC 17978, and XDR A-564 strains. The antibacterial activity of compound **11c** against *A. baumannii* BAA ATCC 747 with a MIC of 20.4 μg mL^{-1} is comparable to that of the commercial antibiotic cefepime (MIC = 15.3 μg mL^{-1}) (Table 1). Furthermore, it was observed that compound **11c** exhibited a MIC value of 61.3 μg mL^{-1} against the XDR A-564 strain, which is better than the MIC value of the reference drug cefepime (MIC > 64 μg mL^{-1}). Nevertheless, it did not show

Table 1 *In vitro* biological data of indolyl-acrylamides **11a–h**, **11a′**, and **12a–j**, MIC and $^{1}HC_{50}$ (μg mL^{-1})

Compounds	*A. b* 17978[a]	*A. b* BAA 747[b]	*A. b* A-564 (XDR)[c]	*P. a* 48-M (MDR)[d]	*K. p* K2 (MDR)[e]	*S. a clinic* (MRSA)[f]	*S. a* 25923[g]	Hemolysis HC_{50}
11a	19.0 ± 1.1*	7.8 ± 1.2*	31.7	>122.2	NT	48.8	>73	≤47
11b	19.7 ± 1.0*	7.5 ± 1.2*	44.3	>110	>66	NT	>66	>40
11c	>61.3	20.4	61.3	>102	NT	>61	>61	>40
11d	>63.5	>21.1	>105.8	>105	>63	>63	>63	NT
11e	>61.5	>61.5	>102.6	>102	>61	>61	>61	NT
11f	>63.9	>63.9	>106.6	>106	>63	>106	>63	>40
11g	8.3 ± 1.0*	3.2 ± 2.3*	10.2 ± 1.1*	46.2	>23	8.9 ± 3.4*	>69	>40
11h	13.7 ± 1.1*	6.3 ± 1.1*	9.6 ± 1.5*	41.7	>20	8.1 ± 1.1*	>62	>40
11a′	>61.6	>41.1	51.3	>102	NT	NT	>61	>40
12a	20.9 ± 1.1*	4.5 ± 1.2*	13.7 ± 1.1*	>114	>22	>22	>68	≤40
12b	8.7 ± 1.1*	8.7 ± 1.0*	31	>103	>20	>20	>62	>40
12c	>56.9	14.2 ± 1.1*	29.6	>94	>56	>18	>56	≤40
12d	>59.0	>59.0	>59.0	>98	>19	>19	>59	NT
12e	**7.1 ± 1.1***	**1.2 ± 2.6***	**4.3 ± 1.1***	23.2 ± 1.1*	12.1 ± 1.2*	**3.2 ± 1.1***	14.2 ± 1.0*	>40
12f	7.4 ± 1.0*	5.9 ± 3.5*	8.8 ± 1.1*	16.3 ± 1.0*	9.7 ± 1.9*	**2.1 ± 2.1***	11.6 ± 1.0*	>40
12g	23.3 ± 1.0*	NT	26.5	>88	>17	>17	>53	>40
12h	15.9 ± 1.1*	9.6 ± 1.1*	37.1	NT	18.5	6.6 ± 1.1*	>55	NT
12i	10.23 ± 1.0*	9.5 ± 1.0*	15.4 ± 1.1*	44.6	>22	6.2 ± 1.2*	21.8 ± 1.0*	<21
12j	8.3 ± 1.1*	**4.4 ± 1.1***	**1.2 ± 1.3***	NT	18.4	8.2 ± 1.9*	16.5 ± 1.9*	>40
Cefepime	16.3	15.3	>64	NT	NT	NT	NT	NT
Meropenem	NT	NT	>32	NT	NT	NT	NT	NT
Gentamicin	0.95	0.95	>64	0.95	0.13	NT	NT	NT
Ciprofloxacin	NT	NT	>50	NT	NT	NT	8	NT
Penicillin G	NT	NT	NT	NT	NT	>84	NT	NT

[a] *A.b*.17978, *Acinetobacter baumannii* ATCC 17978. [b] *A.b*. BAA 747, *Acinetobacter baumannii* ATCC BAA 747. [c] *A.b*. A-564 (XDR), *Acinetobacter baumannii* A-564 (XDR). [d] *P.a*. 48-M (MDR), *Pseudomonas aeruginosa* 48-M (MDR). [e] *K.p*. K2 (MDR), *Klebsiella pneumoniae* K2 (MDR). [f] *S.a*. MRSA, penicillin–methicillin-resistant *Staphylococcus aureus*. [g] *S.a*. ATCC 25923, *Staphylococcus aureus* ATCC 25923.[1]Hemolytic concentration 50 (HC_{50}) (n = 3). *MIC values were calculated with the Gompertz equation using GraphPad Prism 9.5.1, (n = 3). NT = no test.

relevant activity against *A. baumannii* ATCC 17978 (MIC > 61.3 μg mL^{-1}).

Compounds **11a** and **11b**, with a (C5–Br) and (C5–Cl) substituent, respectively, showed better antibacterial activity than cefepime with values of 31.7 and 44.3 μg mL^{-1} respectively against *A. baumannii* XDR A-564 (Table 1). Compound **11a** also showed an MIC of 7.8 μg mL^{-1} against *A. baumannii* BAA ATCC 747, indicating that the bromo substituent at C-5 effectively enhances the antibacterial activity against both strains.[31] The MIC values were 2 times better than those of cefepime for both strains. Likewise, compound **11b** presented a MIC = 7.5 μg mL^{-1} value lower than that of cefepime for strain BAA ATTC 747, but for strain XDR A-564, the potency decreased compared to **11a**.

Based on these results, and aiming to improve the MIC value in the simpler compound **11c** against *A. baumannii* strains, the NH group of the piperazinyl was replaced with O and S, resulting in **11e** and **11f**, respectively.[32] These compounds lost their potency considerably against *A. baumannii* BAA ATCC 747, *A. baumannii* ATCC 17978, and *A. baumannii* XDR A-564, presenting MIC values above 60 μg mL^{-1}.This finding suggested that the NH of the piperazinyl group is crucial for antibacterial potency. This hypothesis was confirmed experimentally by testing compound **11d**, which showed a potency decrease (MIC > 20 μg mL^{-1}) for all strains of *A. baumannii*. Similarly, the double bond influence of the α,β-unsaturated system was evaluated using compound **11a′**. However, the potency was not significantly improved against any strain with a MIC > 40 μg mL^{-1}.

The *N*-2-aminoethyl group was incorporated in compounds with higher activity **11a** and **11b** instead of a piperazinyl moiety to evaluate the influence of the rigidity of the piperazinyl group on bioactivity, generating compounds **11g** (C5–Br) and **11h** (C5–Cl). Compound **11g** showed a significant bioactivity improvement against two ATCC strains of *A. baumannii*, with MIC values of 8.3 μg mL^{-1} for strain 17 978 and 3.2 μg mL^{-1} for strain BAA 747, thus increasing the potency of **11g** two times compared to **11a** against the BAA ATCC 747 strain. Evaluation of compound **11g** against the XDR A-564 strain gave a MIC of 10.2 μg mL^{-1}, indicating that its potency is six times higher than cefepime and three times higher than **11a**. Previous studies have also reported that substituting the indole *N*-linked H with the *p*-Cl-benzyl group enhances the antimicrobial activity.[33] Based on this, replacing the tosyl group with the *p*-Cl-benzyl group and keeping the piperazinyl group and the bromine at C-5 to generate compound **12a** was proposed. Compound **12a** showed a considerable increase in potency against strains BAA 747 and XDR A-564, exhibiting values of 4.5 μg mL^{-1} and 13.7 μg mL^{-1}, respectively, indicating that **12a** presents a significant increase in potency compared to cefepime and compound **11a**. Both structure–activity relationship studies indicate that the *N*-2-aminoethyl group and the *p*-Cl-benzyl group

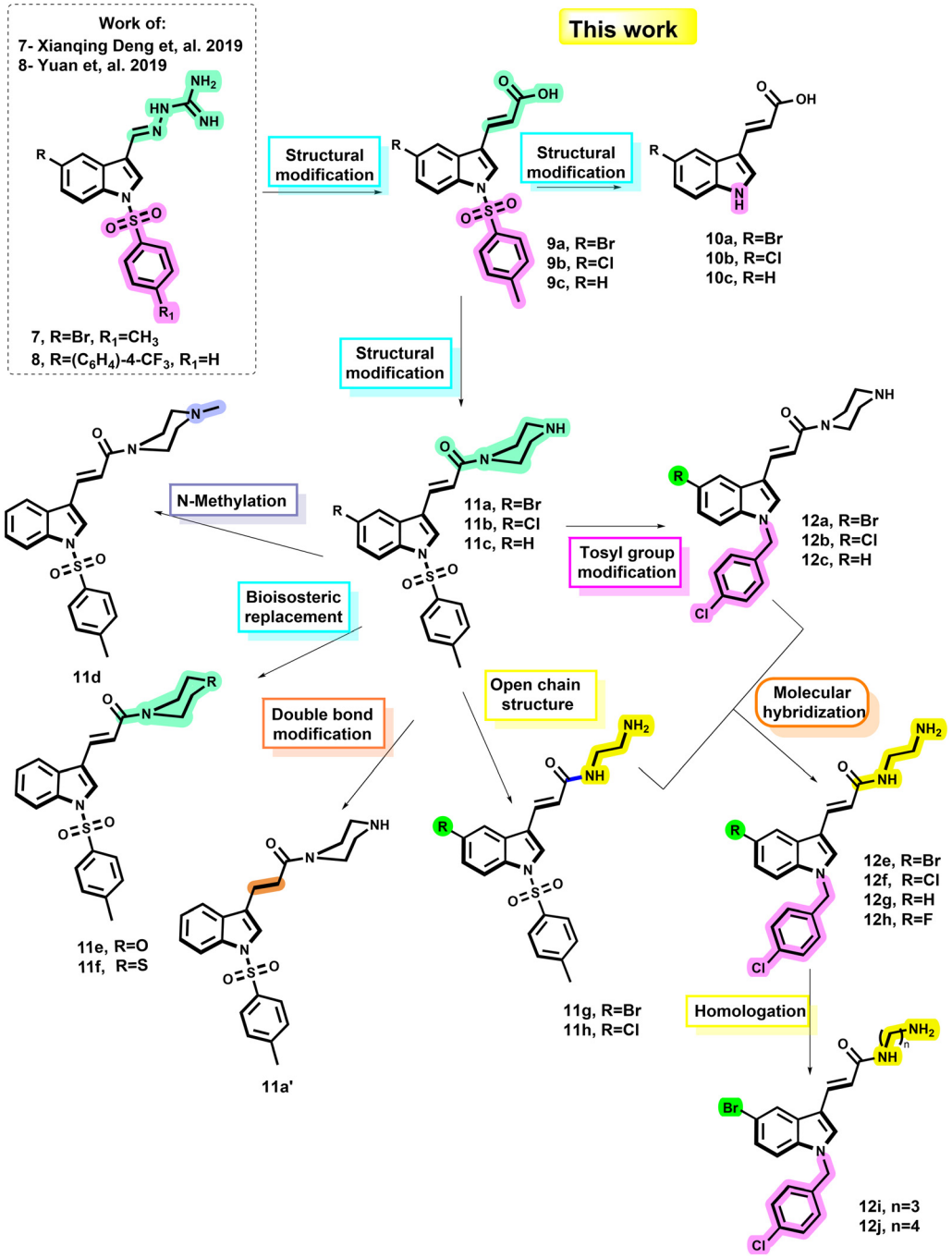

Fig. 2 Rational design of the compounds assessed.

significantly increase the activity against *A. baumannii* strains.

As a consequence, molecular hybridization of both groups in the base structure of the indole ring was proposed, thus obtaining the **12e–h** compounds.[34] Evaluation of compound **12e** (C5–Br) against ATCC strain BAA 747 revealed a MIC value of 1.2 μg mL^{-1}, which is ten times more potent than cefepime. Moreover, this compound showed a remarkable increase in potency against the XDR A-564 with a MIC value of 4.3 μg mL^{-1}, making it thirteen times more potent than cefepime and two times more potent than **11g**, distinguishing **12e** as a promising compound. Subsequently, to improve potency, bromine was retained at carbon 5, and a modification of the chain length (homologation) was proposed, replacing the *N*-2-aminoethyl group with aliphatic chains **12i** $n = 3$ and **12j** $n = 4$.[35] For the *A. baumannii* BAA ATCC 747 strain, compound **12i** showed decreased antibacterial activity with a MIC value of 9.5 μg mL^{-1}. However, for compound **12j**, the MIC was 4.4 μg mL^{-1}, indicating a homologous effect for this strain, with a value

three times better than cefepime. The homology effect against strain XDR A-564 showed the next tendency. Compound **12i** displayed a decrease in potency, with a MIC of 15.4 μg mL^{-1}. At the same time, **12j** showed a homologous effect, with a MIC of 1.2 μg mL^{-1}, representing a significant increase in power compared to **12e**, but a more than 50-fold increase compared to cefepime. In addition, all compounds underwent rigorous testing against other bacteria from the ESKAPEE group, including clinical isolates of penicillin–methicillin-resistant *S. aureus* resulting in very low MIC values of 3.2 μg mL^{-1} with **12e** and of 2.1 μg mL^{-1} with **12f**.

The chemical structure optimization steps and antimicrobial activity results presented in this study demonstrate a procedure that successfully enhanced the biological efficacy of a family of compounds by over tenfold through the derivatization of a privileged core structure. These findings underscore the potential of rational design and targeted structural modifications in drug development, highlighting a promising pathway for the creation of more potent antimicrobial agents. The final lead compounds **12e** and **12j** exhibit significant promise due to their superior bioactivity and potential to address various multidrug-

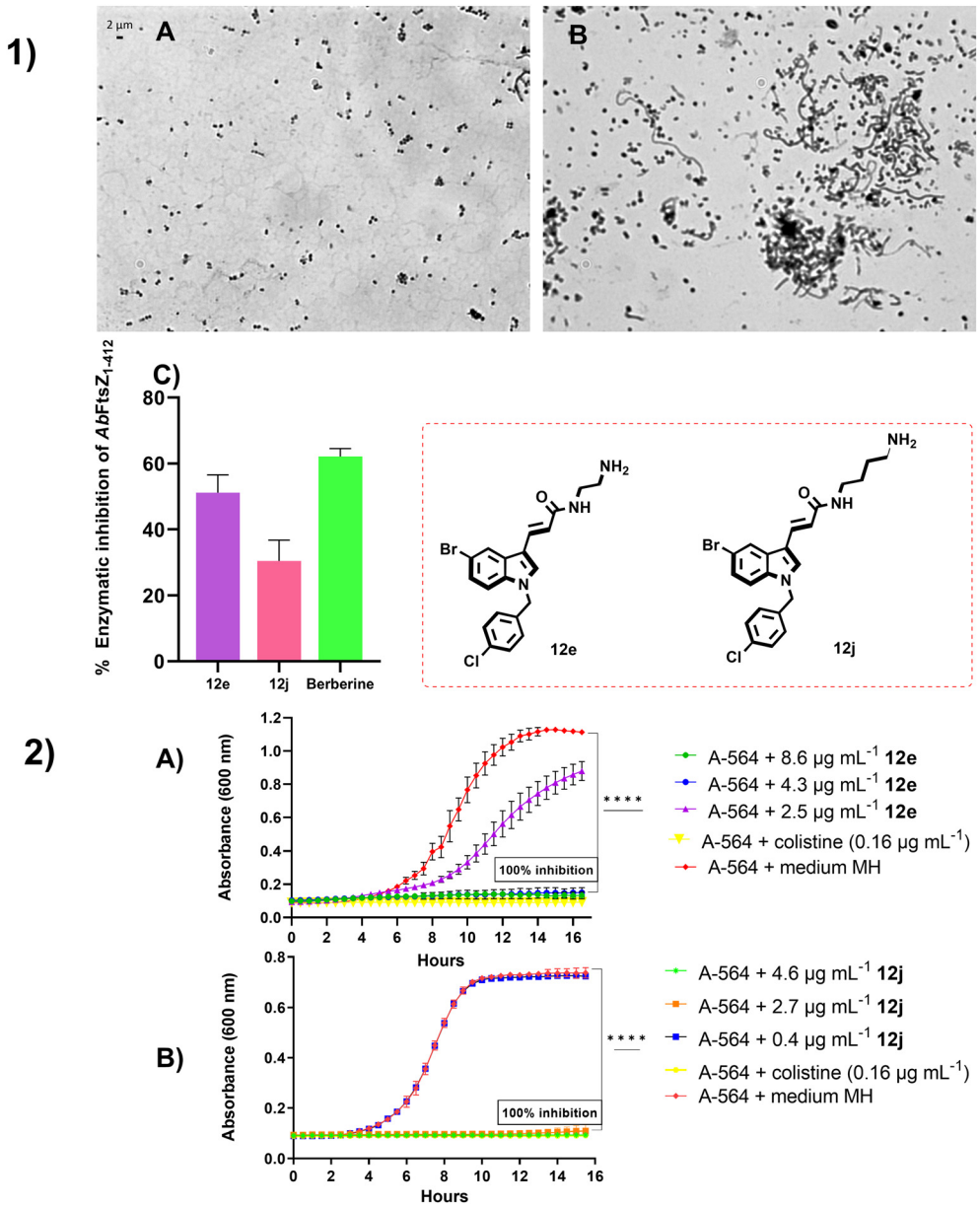

Fig. 3 1) Effects of compound **12e** on the cell morphology of *A. baumannii* XDR A-564 grown in the absence (A) or the presence of 0.5 MIC of **12e** (B). C) Effect of inhibition of GTPase activity of *Ab*$FtsZ_{1-412}$ by indole derivatives **12e** and **12j** (berberine was used as a positive control, 186 μg mL^{-1}, n = 3), 2) growth curves of the strains with the bacterial activity of compounds **12e** (A) and **12j** (B) against *A. baumanii* XDR A-564 (colistin was used as a positive control, n = 3). Three independent experiments were performed, each with three repetitions. The statistical significance was calculated with a t-test in GraphPad 9.5.1.

resistant pathogens, marking a crucial step forward in limiting antimicrobial resistance.

2.4 Morphological effects of the indole family compounds on *A. baumannii* A-564 treated cells

Microscopic observations of the bacterial cell morphology have uncovered a significant finding. At a concentration of 2.1 μg mL^{-1}, **12e** has shown a remarkable effect on *A. baumannii* A-564 cells, increasing their length (B) compared to untreated cells (A) (Fig. 3). This increase in length indicates a potential mechanism causing abnormal bacterial cell division and cell death.[36] The results strongly suggest that the synthesized compound has an inhibitory effect on GTPase activity, leading to instability and abnormal bacterial cell division, ultimately resulting in cell death. These findings could potentially lead to the development of new strategies for combating bacterial infections.

2.5 Effects of indolyl-acrylamides derivatives on the GTPase activity of *Ab*$FtsZ_{1–412}$

The polymerization of the FtsZ protein, a pivotal process for cell division, is intricately linked to the rate of GTP hydrolysis.[37] Previous studies by Carrillo-Jaimes, K. *et al.*,[5] where they expressed and purified the *Ab*$FtsZ_{1–412}$ protein from the XDR A-564 strain, demonstrated that berberine can inhibit the GTPase activity of the *Ab*$FtsZ_{1–412}$ enzymes by no more than 50% at a concentration of 186 μg mL^{-1}. Additionally, other compounds, such as sanguinarine and curcumin,[5] previously reported as FtsZ inhibitors of *E. coli* and *B. subtilis*, were tested but no inhibition was observed for the GTPase activity of *Ab*$FtsZ_{1–412}$. Given the high conservation of this protein in bacterial species, we turned our attention to the potential of **12e** and **12j** to affect the GTPase activity of *Ab*$FtsZ_{1–412}$. This exploration could have far-reaching implications for our understanding of the antibacterial mechanism of indolyl-acrylamides analogs. The compounds were tested in the 8–46 μg mL^{-1} range. In the GTPase assay, **12e** and **12j** demonstrated concentration-dependent inhibition, reaching a maximum inhibition of 51 ± 5.4% and 30.5 ± 6.3% at 32 μg mL^{-1} (Fig. 3).

2.6 Docking and molecular dynamics simulations of compounds 12e (A) and 12j (B) in the GTP binding site of FtsZ

The blind docking study revealed that both compounds strongly prefer the GTP binding site. Additionally, both compounds showed a highly similar binding mode at this site, depicted in gray (Fig. 4). Three independent 100 ns MD simulations showed that the protein backbone remained stable with an RMSD of less than 0.25 nm. However, both

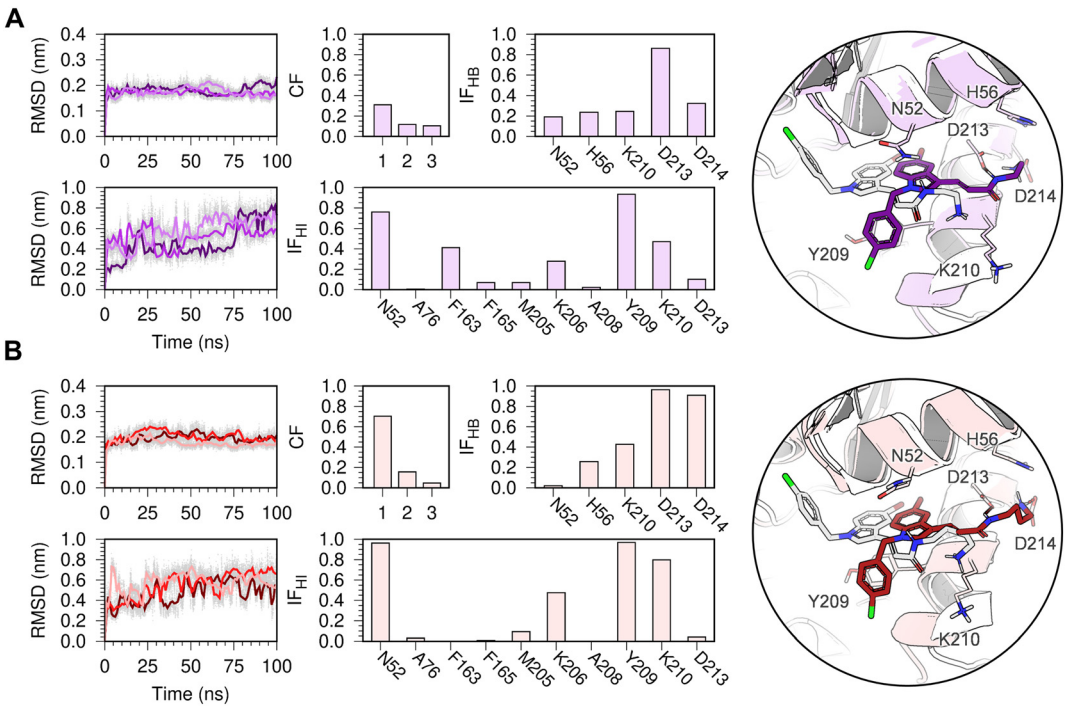

Fig. 4 Docking and molecular dynamics results of (A) **12e** and (B) **12j**. The left plots depict the backbone (top) and ligand (top) RMSD after least squares fit to the protein backbone for the three independent MD simulations. Histogram plots show the fraction of structures within the first three clusters (CF) and the fraction of hydrogen bond (IFHB) and hydrophobic (IFHI) interactions between the compounds and the protein. These fractions were obtained from the combined analysis of the three MD replicas. The figures on the right illustrate the docking pose with the highest score (gray) and the most representative pose from the MD simulations (purple and red, respectively), along with the residues with which they interacted most during the MD simulations.

ligands exhibited a significant change in orientation at the site compared to the predicted docking pose. By analyzing the fraction of structures derived from clustering analysis (CF), the most representative pose for each ligand was identified. One of the most intriguing findings of our study is the unexpected similarity in the poses of both ligands. Despite this, the pose of compound **12e** was only represented in 31.0% of the last 50 ns across the three simulations, while compound **12j**'s binding pose, despite its longer aliphatic chain, was found in 70.4%. Both compounds also exhibited highly similar profiles of hydrogen bond (HB) and hydrophobic (HI) interaction fractions (IFs). They formed hydrogen bonds with D213 in over 80.0% of the replicas, as well as a high percentage of hydrophobic contacts with N52 and Y209. Compound **12j** also formed a hydrogen bond with D214 and hydrophobic interactions with K210 during the simulations. Despite these similarities, compound **12j** may exhibit lower FtsZ inhibitory activity due to the potential increase in conformational entropy caused by its longer chain, which could affect its binding affinity.

2.7 Effect of indolyl-acrylamides on membrane permeabilization

Previous studies have shown that specific FtsZ inhibitors can induce secondary effects on the bacterial membrane, leading to cell lysis.[38] In *A. baumannii*, membrane disruption is a particularly relevant mechanism, given that this bacterium possesses a highly impermeable outer membrane that confers resistance to multiple antibiotics.[39] The cell viability assay (Fig. 5) revealed that bacteria treated with **12e** and **12j** exhibited more dead cells (stained red) than the untreated control, in which no dead cells were observed. Moreover, in bacteria exposed to **12e**, virtually no live cells (stained green) were detected. These results indicate that cells treated with these compounds showed increased permeability to propidium iodide (PI) (Fig. 5), suggesting that both compounds compromise the stability of the *A. baumannii* A-564 membrane, as PI is a marker that only penetrates damaged membranes.

2.8 Hemolysis

Hemolysis, the breakdown of red blood cells, can be caused by exogenous factors and lead to health complications. The hemolysis assay, a tool that can be used to evaluate the safety and usefulness of new compounds with promising biological activity, has shown promising results.[40,41] All compounds were tested at 40 μg mL^{-1}. Interestingly, the hemolytic properties of the most active compounds against *A. baumannii* XDR A-564 and *A. baumannii* BAA ATCC 747, **12e** and **12j**, were >40 μg mL^{-1} (Fig. 6), indicating that the compounds present more selectivity against microorganisms with a lower effect on red blood cells.

3. Conclusions

In summary, a novel library of indolyl-acrylamides analogs was synthesized by an *in vitro* MIC activity-guided structure–activity relationship (SAR) study, and their *in vitro* antibacterial activity was evaluated. The results show that these compounds exhibit up to ten fold increased potency against resistant and extremely resistant bacteria when they present the following structural features: 1) a bromo bonded at the C-5 position of the indole ring, 2) a *p*-chlorobenzyl group joined to indole nitrogen, 3) an increase in the rotational degrees of freedom of the *N*-amino group bonded

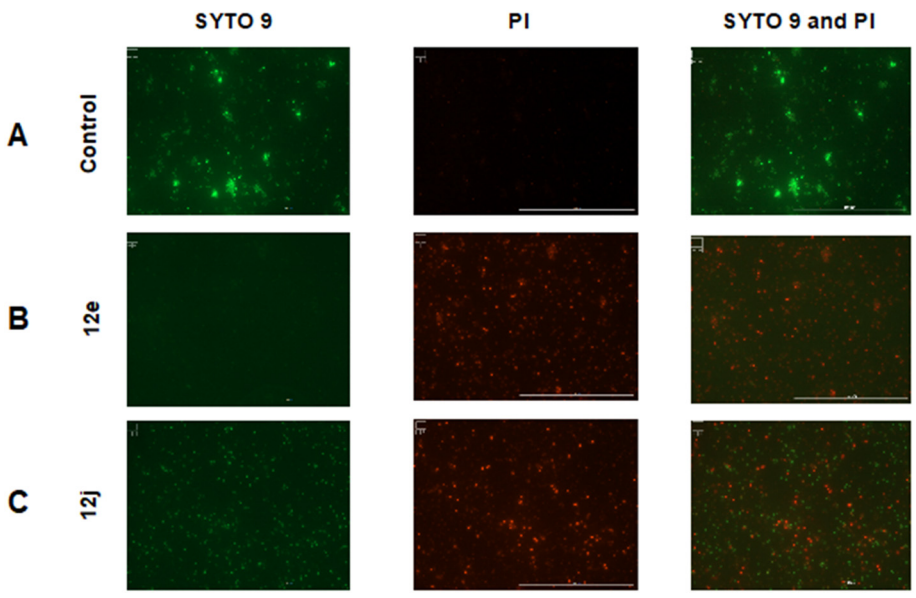

Fig. 5 Fluorescence microscopy of live and dead *A. baumannii* A-564 cells treated with compounds. (A) Untreated control cells. Most appear green, indicating viability. (B) and (C) Cells treated with compounds **12e** and **12j** (2× MIC), respectively. Scale bar: 100 μm.

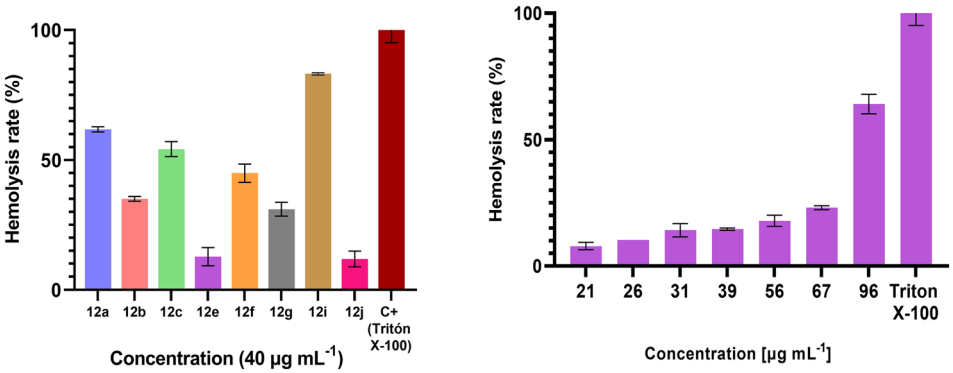

Fig. 6 The hemolysis rates of rabbit red blood cells induced by **12a**–**12j** compounds, and **12e** at different concentrations, Triton X-100 was used as a positive control. Three independent experiments were performed, each with three repetitions (n = 3).

to the C-1 carbonyl moiety, and 4) a homology effect due to chain length. Significant antibacterial activity against various strains, including those multidrug-resistant, was obtained with these modifications (Fig. 7). Importantly, the antibacterial activities observed against *A. baumannii* A-564 XDR ranged from 4.3 μg mL^{-1} to 1.2 μg mL^{-1}, significantly lower compared to that of cefepime (MIC > 64 μg mL^{-1}), among others. Furthermore, our research has uncovered compounds demonstrating potent antibacterial activity against methicillin-resistant *S. aureus* (MRSA), with compounds **12e** and **12f** emerging as standout performers with MIC values of 3.2 μg mL^{-1} and 2.1 μg mL^{-1}, respectively. The MIC values of several of these compounds are equally promising against Gram-negative strains, such as drug-resistant *K. pneumoniae* and *P. aeruginosa*, suggesting a common cellular target or multiple mechanisms of action. These findings, coupled with additional biochemical evaluations that reveal at least one mode of action of these compounds, suggest a potential breakthrough. Furthermore, compounds **12e** and **12j** have demonstrated the potential to inhibit 50% of the enzymatic activity of *Ab*FtsZ$_{1-412}$. Notably, both compounds were able to inhibit *A. baumannii* growth at concentrations lower than those required to inhibit *Ab*FtsZ$_{1-412}$, suggesting the involvement of additional mechanisms in their antibacterial effect and, consequently, in their antimicrobial activity. The ability of **12e** and **12j** to disrupt membrane integrity could represent an additional mechanism enhancing their efficacy against *A. baumannii*. Importantly, **12e** and **12j** exhibited negligible hemolytic activity compared to their MIC values against *A. baumannii* strains, suggesting a possible selectivity for prokaryotic membranes. Antimicrobials with multiple mechanisms of action offer significant advantages in combating antimicrobial resistance (AMR). They reduce the likelihood of resistance development by targeting multiple pathways, enhance efficacy and provide broad-spectrum activity against a range of pathogens, including MDR and XDR strains. By effectively targeting resistant strains, these antimicrobials also help mitigate the spread of resistance genes, contributing to better long-term control of AMR. This multifaceted approach represents a promising strategy for developing more effective and sustainable treatments. However, further studies are needed to fully understand the factors driving this selective interaction with bacterial membranes. The implications of these findings are profound, suggesting that novel indolyl-acrylamides could be a beacon of hope in the fight against drug-resistant bacteria.

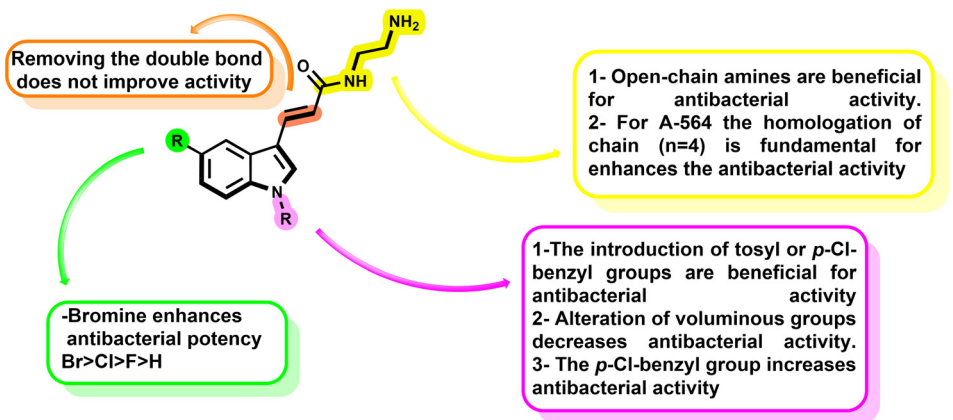

Fig. 7 Brief of the structure–activity relationship of evaluated compounds.

4. Biological assay

4.1 Antibacterial assay

The antimicrobial activities of compounds **9a–c**, **10a–c**, **11a–h**, **11a′**, and **12a–j** were evaluated according to the method described in CLSI guidelines M07-A10 (microdilution assay) (CLSI 2015).[42] The bacterial strain was suspended in Müller–Hinton broth at 37 °C for 12 h, and turbidity was adjusted to 0.5 McFarland standard units (108 CFU mL^{-1}) equivalent to 0.08–0.13 optical density units (600 nm). Molecules were evaluated at concentrations between 0.1 and 250 μM dissolved in DMSO. The microdilution setup consisted of 10 μL of bacterial suspension, 2 μL of sample (compounds), and 88 μL of Müller–Hinton broth. The optical density of the plate was then measured at 600 nm (OD600) using a BioTek Cytation 7 cell imaging multimode reader plate reader. The plate was then incubated at 37 °C for 24 h, and the measurement was repeated to calculate the % inhibition and growth rate. The % inhibition was calculated using eqn (1), and the minimum inhibitory concentrations of the compounds were calculated by nonlinear regression using a modified Gompertz function with GraphPad Prism 9.5.1.[5,42]

$$\%\ \text{Bacterial inhibition} = \left(1 - \frac{\text{Abs}_{\text{compound } t=24\text{h}} - \text{Abs}_{\text{compound } t=0\text{h}}}{\text{Abs}_{\text{negative control } t=24\text{h}} - \text{Abs}_{\text{negative control } t=0\text{h}}}\right) \times 100 \quad (1)$$

4.2 Microscopic visualization

Cells of strain *A. baumannii* A-564 were grown in Müller–Hinton medium and incubated for 24 h, then the bacterial culture was re-suspended in Müller–Hinton broth, and the turbidity was adjusted to 0.5 McFarland standard units (108 CFU mL^{-1}) equivalent to 0.08–0.13 optical density units (600 nm). The microdilution setup consisted of 10 μL of bacterial suspension, 2 μL of **12e** (in DMSO), and 88 μL of Müller–Hinton broth; in 4 wells of the plate, there was no compound and in 4 other wells, the 0.5 MIC of the test compound was cultured at 37 °C for 24 h. Cells for morphology studies were collected and stained with Gram stain. Images were captured using a Zeiss Imager.M2 microscope with an Axiocam 503.2 camera.[36]

4.3 Hemolysis assay

Rabbit erythrocytes were resuspended in 0.9% w/v NaCl and centrifuged at 3000 × *g* for 10 minutes. This procedure was repeated until a clear supernatant was obtained. The erythrocytes were then resuspended in a 50 mM phosphate buffer, pH 7.4, containing 150 mM NaCl to prepare a 20% v/v solution. For the assay, 96-well flat-bottom microplates were used. Each well was loaded with 50 μL of buffer, 50 μL of erythrocytes, and 2 μL of each compound to be tested (diluted in DMSO), to achieve a final volume of 102 μL per well. The plates were incubated for 4 h at 37 °C. After incubation, 25 μL of the supernatant was transferred to a new plate, and absorbance was measured at 405 nm using a BioTek Cytation 7 cell imaging multimode reader.[43] All experiments were performed in triplicate, using Triton X-100 as a positive control and DMSO as a negative control. Compounds were tested at a concentration of 40 μg mL^{-1}, and the percentage of hemolysis was calculated using the following formula:

$$\%\ \text{hemolysis} = \left(\frac{\text{Abs}_{\text{compound}} - \text{Abs}_{\text{negative control}}}{\text{Abs}_{\text{positive control}} - \text{Abs}_{\text{negative control}}}\right) \times 100 \quad (2)$$

4.4 Enzymatic assay of *Ab*FtsZ$_{1-412}$

The evaluation of enzyme inhibition was performed following a protocol reported.[5] The assay was performed in a 96-well plate, employing a buffer solution of 50 mM Tris, 200 mM KCl, and 2.5 mM $MgCl_2$ at pH 7.0, GTP as a substrate (50 μM), *Ab*FtsZ$_{1-412}$ enzyme (4 μM) and **12e** and **12j** to be evaluated (20–100 μM in DMSO). Then, the plate was incubated for 30 min at 37 °C; after this time, a malachite green solution (malachite green 79%, molybdate 20%, Tween 1%) was added, and then the absorbance was read at 630 nm using a BioTek Cytation 7 cell imaging multimode plate reader. All experiments were performed in triplicate, using berberine (500 μM) as a positive control and DMSO as a negative control. The activity results were calculated with eqn (3) and are expressed as a percentage (%).

$$\%\ \text{FtsZ inhibition} = \left(\frac{\text{Abs}_{\text{compound}}}{\text{Abs}_{\text{negative control}}}\right) \times 100 \quad (3)$$

4.5 Cell viability assay LIVE/DEAD

The cell viability of the *A. baumannii* XDR strain A-564 was assessed using a LIVE/DEAD BacLight Bacterial Viability Kit, following the manufacturer's instructions (Thermo Fisher Scientific, MA, USA). Bacterial cultures were grown to the late log phase, then centrifuged at 5000 × *g* and resuspended in 2 mL of culture medium to achieve an OD_{600} of 5. The cells were transferred to a 96-well plate and exposed to twice the MIC of compounds **12e** and **12j** for 6 hours at 37 °C in 100 μL reaction volume. Following treatment, cultures—including the untreated negative control—were harvested and washed with 0.85% NaCl by centrifugation at 10 000 × *g* for 10 minutes at 4 °C. The cell pellet was resuspended in 0.85% NaCl, and a fluorescent nucleic acid stain mixture containing SYTO 9 and propidium iodide (PI) was added. SYTO 9 penetrates all cells, regardless of membrane integrity, binds to nucleic acids, and fluoresces green. In contrast, PI only crosses damaged bacterial membranes, binding to nucleic acids and fluorescing red, thus serving as a marker of membrane integrity. Stained cells were incubated at room temperature for 15 minutes in the dark with constant shaking. Fluorescence analysis was performed using a BioTek Cytation 5 multimode cell imaging reader (Agilent) equipped with a 40× objective and filters for fluorescein and Texas Red.

Image processing was carried out using BioTek Gen5 Software (Agilent) for imaging and microscopy.

5. Docking and molecular dynamics simulations of compounds **12e** and **12j** in the GTP site of FtsZ

5.1 Ligand preparation

The tridimensional structures of compounds **12e** and **12j** were generated from the SMILES representation using the OpenBabel toolbox.[44] Both compounds underwent energy minimization using the Universal Force Field (UFF) implemented in the same software. Subsequently, a second round of geometry optimization and energy minimization was conducted with Gaussian 16,[45] using the B3LYP[46,47] density functional and the 6-31G(d) basis set.

5.2 Protein preparation

A homology model of the FtsZ protein from *A. baumannii* was constructed using the SwissModel web server.[48] We employed the FtsZ crystal structure from *Pseudomonas aeruginosa* (PDB ID: 1OFU, resolution: 2.10 Å) as the template for our model. This structure was chosen as the template since it had the highest sequence identity with the FtsZ sequence from *A. baumannii*, based on the BLAST analysis conducted in UniProt[49] with the UniProtKB with the 3D structure target database. The assessment of the generated structure showed that the model has acceptable global model quality estimate (GMQE) and QMEANDisCo global scores,[50] with values of 0.64 and 0.78, respectively. Additionally, the Ramachandran plot indicated that 96.38% of the backbone dihedral angles are in the favored region. MolProbity[51] revealed no Cβ deviations or bad bonds and only 10 bad angles, and only 3.77% of residues were identified as rotamer outliers.

5.3 Molecular docking

To identify the most reliable binding site and binding mode of both **12e** and **12j** in *Ab*FtsZ, we carried out a blind docking study using QuickVina-W.[52] We set a search box covering the entire surface of the structure and an exhaustiveness value of 50 for the docking to ensure thorough exploration. From the 20 docking runs, we selected the binding pose with the best score for the molecular dynamics simulations.

5.4 Molecular dynamics

The selected binding poses of compounds **12e** and **12j** within the GTP site of *Ab*FtsZ were subjected to three independent 100 ns molecular dynamics (MD) simulations using the AMBER14SB[53] force field in GROMACS 2021.[54] The ACPYPE package[55] was used to parametrize the molecules within the AMBER force field framework and generate the necessary GROMACS input files. To carry out the MD simulations, the protein–ligand complexes were initially solvated in a cubic box using the TIP3P water model. Sodium and chloride ions were added randomly to neutralize the system and achieve a concentration of 0.15 M. Subsequently, an energy minimization step was applied, followed by a 1 ns equilibration period in both the canonical (NVT) and isothermal–isobaric (NPT) ensembles. Once equilibrated, the system underwent a 100 ns non-restrained NPT production run. The temperature was maintained at 300 K using the V-rescale algorithm,[56] while the pressure was controlled at 1.0 bar using the Parrinello-Rhaman barostat.[57] All hydrogen-containing bonds were constrained using the LINCS algorithm.[58] Additionally, a Lennard–Jones potential with a shift function was employed within a range of 1.0 to 1.2 nm, while electrostatic interactions were computed within a 1.2 nm cutoff radius. Long-range electrostatic interactions were calculated using the PME method.[59]

Here, the root-mean-square deviation (RMSD) of the *Ab*FtsZ backbone and ligand heavy atoms after least squares fit to the protein backbone were computed for each MD simulation replica. The last 50 ns of the three MD replicas were collectively analyzed, determining the most representative pose of the compounds using a ligand RMSD-based clustering analysis with a cutoff value of 0.2 nm and employing the Gromos method. The number of hydrogen bonds and hydrophobic interactions formed during the simulations was also computed using the GROMACS-built in tools and the stand-alone application of PLIP v2.3.0.[60] Figures and plots were generated using PyMOL[61] and Gnuplot,[62] respectively.

Data availability

The data supporting this article have been included as part of the ESI.†

Author contributions

Velvett G. Domínguez-Méndez: investigation, methodology, writing; Rosa Ma. Chávez Santos: investigation, methodology; Karol Carrillo-Jaimes: data curation, investigation, methodology, writing – original draft; Alejandra Hernández-Santoyo: methodology, investigation; Santos Ramírez-Carreto: methodology, writing; Armando Hernández-Garcia: methodology, visualization, writing; Rodrigo Aguayo-Ortiz: investigation, methodology, software, supervision, writing – review & editing; Corina-Diana Ceapă: conceptualization, formal analysis, investigation, methodology, visualization, writing review and editing, Corina-Diana Ceapă: conceptualization, formal analysis, investigation, methodology, visualization, writing – review and editing; José Rivera-Chávez: data curation, formal analysis, methodology, supervision and writing – review and editing; Roberto Martínez: project administration, funding acquisition, conceptualization, supervision, and writing – review and editing.

Conflicts of interest

The authors declare that they have no known competing financial interests or personal relationships that could have appeared to influence the work reported in this paper.

Acknowledgements

We acknowledge financial support from DGAPA-UNAM (grant IN204619). The work of AHG and SRC has been supported by UNAM-PAPIIT IN226624. VGDM thanks SECIHTI for a PhD fellowship (CVU 963609), SRC thanks UNAM-DGAPA for the postdoctoral fellowship awarded (period: October 2024–September 2025). RMCS thanks SECIHTI for the postdoctoral fellowship awarded (period: September 2023–August 2025), (CVU: 269079). We are also grateful for the technical support provided by Carmen Garcia, Angeles Peña, Javier Perez, Elizabeth Huerta, Isabel Chavez, Teresa Ramirez Apan and Antonio Nieto Camacho (IQ-UNAM).

References

1 C. J. Iwu-Jaja, A. Jaca and I. F. Jaja, *et al.*, Preventing and managing antimicrobial resistance in the African region: A scoping review protocol, *PLoS One*, 2021, **16**, e0254737.
2 C. J. L. Murray, K. S. Ikuta and F. Sharara, *et al.*, Global burden of bacterial antimicrobial resistance in 2019: a systematic analysis, *Lancet*, 2022, **399**, 629–655.
3 T. R. Walsh, A. C. Gales, R. Laxminarayan and P. C. Dodd, Antimicrobial Resistance: Addressing a Global Threat to Humanity, *PLoS Med.*, 2023, **20**, e1004264.
4 S. Ruekit, A. Srijan and O. Serichantalergs, *et al.*, Molecular characterization of multidrug-resistant ESKAPEE pathogens from clinical samples in Chonburi, Thailand (2017-2018), *BMC Infect. Dis.*, 2022, **22**, 695.
5 K. Carrillo-Jaimes, C. A. Fajardo-Hernández and F. Hernández-Sedano, *et al.*, Antibacterial Activity and AbFtsZ Binding Properties of Fungal Metabolites Isolated from Mexican Mangroves, *Rev. Bras. Farmacogn.*, 2024, **34**, 564–576.
6 WHO publishes list of bacteria for which new antibiotics are urgently needed **https://www.who.int/news/item/27-02-2017-who-publishes-list-of-bacteria-for-which-new-antibiotics-are-urgently-needed** (accessed Oct 16, 2024).
7 M. Y. Cruz-Muñiz, L. E. López-Jacome and M. Hernández-Durán, *et al.*, Repurposing the anticancer drug mitomycin C for the treatment of persistent *Acinetobacter baumannii* infections, *Int. J. Antimicrob. Agents*, 2017, **49**, 88–92.
8 R. W. DeSimone, K. S. Currie, S. A. Mitchell, J. W. Darrow and D. A. Pippin, Privileged structures: applications in drug discovery, *Comb. Chem. High Throughput Screening*, 2004, **7**(5), 473–494.
9 F. R. de Sá Alves, E. J. Barreiro and C. A. M. Fraga, From nature to drug discovery: the indole scaffold as a "privileged structure", *Mini-Rev. Med. Chem.*, 2009, **9**, 782–793.
10 N. Chadha and O. Silakari, Indoles as therapeutics of interest in medicinal chemistry: Bird's eye view, *Eur. J. Med. Chem.*, 2017, **134**, 159–184.
11 X. Rabasseda, Ramosetron, a 5-HT3 receptor antagonist for the control of nausea and vomiting, *Drugs Today*, 2002, **38**, 75–89.
12 Subcutaneous Sumatriptan International Study Group, Treatment of Migraine Attacks with Sumatriptan, *N. Engl. J. Med.*, 1991, **325**, 316–321.
13 G. D. Morse, R. C. Reichman and M. A. Fischl, *et al.*, Concentration-targeted phase I trials of atevirdine mesylate in patients with HIV infection: dosage requirements and pharmacokinetic studies, *Antiviral Res.*, 2000, **45**, 47–58.
14 T. Vedekhina, A. Lukin, E. Rogacheva, L. Kraeva and M. Krasavin, Zn(OTf)2-catalyzed arenehydrazination of protected propargylamines leading to 3-amidoindoles, *Tetrahedron Lett.*, 2020, **61**, 151430.
15 J. Brem, T. Panduwawala and J. U. Hansen, *et al.*, Imitation of β-lactam binding enables broad-spectrum metallo-β-lactamase inhibitors, *Nat. Chem.*, 2022, **14**, 15–24.
16 M. F. Richter, B. S. Drown and A. P. Riley, *et al.*, Predictive compound accumulation rules yield a broad-spectrum antibiotic, *Nature*, 2017, **545**, 299–304.
17 M. Song, S. Wang and Z. Wang, *et al.*, Synthesis, antimicrobial and cytotoxic activities, and molecular docking studies of N-arylsulfonylindoles containing an aminoguanidine, a semicarbazide, and a thiosemicarbazide moiety, *Eur. J. Med. Chem.*, 2019, **166**, 108–118.
18 W. Yuan, Z. Yu and W. Song, *et al.*, Indole-core-based novel antibacterial agent targeting FtsZ, *Infect. Drug Resist.*, 2019, **12**, 2283–2296.
19 N. Sun, Y.-Y. Zheng and R.-L. Du, *et al.*, New application of tiplaxtinin as an effective FtsZ-targeting chemotype for an antimicrobial study, *MedChemComm*, 1909, **2017**, 8.
20 X. Yang, Z. Lyu and A. Miguel, *et al.*, GTPase activity–coupled treadmilling of the bacterial tubulin FtsZ organizes septal cell wall synthesis, *Science*, 2017, **355**, 744–747.
21 A. W. Bisson-Filho, Y.-P. Hsu and G. R. Squyres, *et al.*, Treadmilling by FtsZ filaments drives peptidoglycan synthesis and bacterial cell division, *Science*, 2017, **355**, 739–743.
22 R. R. Battaje, R. Piyush, V. Pratap and D. Panda, Models versus pathogens: how conserved is the FtsZ in bacteria?, *Biosci. Rep.*, 2023, **43**, BSR20221664.
23 Y. Qiao, T. Si, M.-H. Yang and R. A. Altman, Metal-Free Trifluoromethylation of Aromatic and Heteroaromatic Aldehydes and Ketones, *J. Org. Chem.*, 2014, **79**, 7122–7131.
24 P. Guo, W. Sun and Y. Liu, *et al.*, Stereoselective Synthesis of Vinylcyclopropa[b]indolines via a Rh-Migration Strategy, *Org. Lett.*, 2020, **22**, 5978–5983.
25 Q. Xu, L. Huang and J. Liu, *et al.*, Design, synthesis and biological evaluation of thiazole- and indole-based derivatives for the treatment of type II diabetes, *Eur. J. Med. Chem.*, 2012, **52**, 70–81.
26 S. J. Taylor, A. K. Padyana and A. Abeywardane, *et al.*, Discovery of potent, selective chymase inhibitors via

fragment linking strategies, *J. Med. Chem.*, 2013, **56**, 4465–4481.
27 G. Jin, S. Lee and M. Choi, *et al.*, Chemical genetics-based discovery of indole derivatives as HCV NS5B polymerase inhibitors, *Eur. J. Med. Chem.*, 2014, **75**, 413–425.
28 CLSI, Methods for Antimicrobial Susceptibility Test for Bacteria That Grow Aerobically Approved Standard-Eight Edition, CLSI document M07-A8, Clinical and Laboratory Standards Institute, Wayne, PA, 2009.
29 S. Kumar Verma, R. Verma and F. Xue, *et al.*, Antibacterial activities of sulfonyl or sulfonamide containing heterocyclic derivatives and its structure-activity relationships (SAR) studies: A critical review, *Bioorg. Chem.*, 2020, **105**, 104400.
30 S. Mazzotta, T. Cebrero-Cangueiro and L. Frattaruolo, *et al.*, Exploration of piperazine-derived thioureas as antibacterial and anti-inflammatory agents. *In vitro* evaluation against clinical isolates of colistin-resistant *Acinetobacter baumannii*, *Bioorg. Med. Chem. Lett.*, 2020, **30**, 127411.
31 F. Song, Z. Li and Y. Bian, *et al.*, Indole/isatin-containing hybrids as potential antibacterial agents, *Arch. Pharm.*, 2020, **353**, 2000143.
32 P. Liu, Y. Jiang and L. Jiao, *et al.*, Strategies for the Discovery of Oxazolidinone Antibacterial Agents: Development and Future Perspectives, *J. Med. Chem.*, 2023, **66**, 13860–13873.
33 W. Hong, J. Li and Z. Chang, *et al.*, Synthesis and biological evaluation of indole core-based derivatives with potent antibacterial activity against resistant bacterial pathogens, *J. Antibiot.*, 2017, **70**, 832–844.
34 C. Zeng, S. R. Avula, J. Meng and C. Zhou, Synthesis and Biological Evaluation of Piperazine Hybridized Coumarin Indolylcyanoenones with Antibacterial Potential, *Molecules*, 2023, **28**, 2511.
35 G. Bahatheg, R. Kuppusamy and M. Yasir, *et al.*, Short Tryptamine-Based Peptoids as Potential Therapeutics for Microbial Keratitis: Structure-Function Correlation Studies, *Antibiotics*, 2022, **11**, 1074.
36 N. Sun, R.-L. Du and Y.-Y. Zheng, *et al.*, Antibacterial activity of N-methylbenzofuro[3,2-b]quinoline and N-methylbenzoindolo[3,2-b]-quinoline derivatives and study of their mode of action, *Eur. J. Med. Chem.*, 2017, **135**, 1–11.
37 L. Carro, Recent Progress in the Development of Small-Molecule FtsZ Inhibitors as Chemical Tools for the Development of Novel Antibiotics, *Antibiotics*, 2019, **8**, 217.
38 D. A. Ramirez-Diaz, A. Merino-Salomón and F. Meyer, *et al.*, FtsZ induces membrane deformations via torsional stress upon GTP hydrolysis, *Nat. Commun.*, 2021, **12**, 3310.
39 F. Perez, A. M. Hujer and K. M. Hujer, *et al.*, Global Challenge of Multidrug-Resistant Acinetobacter baumannii, *Antimicrob. Agents Chemother.*, 2007, **51**, 3471–3484.
40 I. P. Sæbø, M. Bjørås, H. Franzyk, E. Helgesen and J. A. Booth, Optimization of the Hemolysis Assay for the Assessment of Cytotoxicity, *Int. J. Mol. Sci.*, 2023, **24**, 2914.
41 N. Liaqat, N. Jahan, K. ur Rehman, T. Anwar and H. Qureshi, Green synthesized silver nanoparticles: Optimization, characterization, antimicrobial activity, and cytotoxicity study by hemolysis assay, *Front. Chem.*, 2022, **10**, 952006.
42 R. J. W. Lambert and J. Pearson, Susceptibility testing: accurate and reproducible minimum inhibitory concentration (MIC) and non-inhibitory concentration (NIC) values, *J. Appl. Microbiol.*, 2000, **88**, 784–790.
43 S. A. Li, R. J. Zheng and K. Sue, *et al.*, Discovery and Preliminary Structure-Activity Investigation of 3-Substituted-1H-imidazol-5-yl-1H-indoles with In Vitro Activity towards Methicillin-Resistant Staphylococcus aureus, *Antibiotics*, 2022, **11**, 1450.
44 N. M. O'Boyle, M. Banck and C. A. James, *et al.*, Open Babel: An open chemical toolbox, *Aust. J. Chem.*, 2011, **3**, 33.
45 M. J. Frisch, G. W. Trucks and H. B. Schlegel, *et al.*, *Gaussian 16, Revision A.03*, Gaussian, Inc., Wallingford, CT, 2016.
46 C. Lee, W. Yang and R. G. Parr, Development of the Colle-Salvetti correlation-energy formula into a functional of the electron density, *Phys. Rev. B: Condens. Matter Mater. Phys.*, 1988, **37**, 785–789.
47 A. D. Becke, Density-functional thermochemistry. III. The role of exact exchange, *J. Chem. Phys.*, 1993, **98**, 5648–5652.
48 A. Waterhouse, M. Bertoni and S. Bienert, *et al.*, SWISS-MODEL: Homology modelling of protein structures and complexes, *Nucleic Acids Res.*, 2018, **46**, W296–W303.
49 A. Bateman, M.-J. Martin and S. Orchard, *et al.*, UniProt: the universal protein knowledgebase in 2021, *Nucleic Acids Res.*, 2021, **49**, D480–D489.
50 G. Studer, C. Rempfer and A. M. Waterhouse, *et al.*, QMEANDisCo—distance constraints applied on model quality estimation, *Bioinformatics*, 2020, **36**, 1765–1771.
51 C. J. Williams, J. J. Headd and N. W. Moriarty, *et al.*, MolProbity: More and better reference data for improved all-atom structure validation, *Protein Sci.*, 2018, **27**, 293–315.
52 N. M. Hassan, A. A. Alhossary, Y. Mu and C. K. Kwoh, Protein-Ligand Blind Docking Using QuickVina-W with Inter-Process Spatio-Temporal Integration, *Sci. Rep.*, 2017, **7**, 1–13.
53 J. A. Maier, C. Martinez and K. Kasavajhala, *et al.*, ff14SB: Improving the Accuracy of Protein Side Chain and Backbone Parameters from ff99SB, *J. Chem. Theory Comput.*, 2015, **11**, 3696–3713.
54 M. J. Abraham, T. Murtola and R. Schulz, *et al.*, GROMACS: High performance molecular simulations through multi-level parallelism from laptops to supercomputers, *SoftwareX*, 2015, 19–25.
55 A. W. Sousa da Silva and W. F. Vranken, ACPYPE - AnteChamber PYthon Parser interfacE, *BMC Res. Notes*, 2012, **5**, 367.
56 G. Bussi, D. Donadio and M. Parrinello, Canonical sampling through velocity rescaling, *J. Chem. Phys.*, 2007, **126**, 1–7.

57 M. Parrinello and A. Rahman, Strain fluctuations and elastic constants, *J. Chem. Phys.*, 1982, **76**, 2662–2666.
58 B. Hess, H. Bekker, H. J. C. Berendsen and J. G. E. M. Fraaije, LINCS: A linear constraint solver for molecular simulations, *J. Comput. Chem.*, 1997, **18**, 1463–1472.
59 T. Darden, D. York and L. Pedersen, Particle mesh Ewald: An N·log(N) method for Ewald sums in large systems, *J. Chem. Phys.*, 1993, **98**, 10089.
60 M. F. Adasme, K. L. Linnemann and S. N. Bolz, *et al.*, PLIP 2021: expanding the scope of the protein–ligand interaction profiler to DNA and RNA, *Nucleic Acids Res.*, 2021, **49**, W530–W534.
61 L. Schrödinger, *The PyMOL Molecular Graphics System, Version 2.5.4*, Schrödinger, LLC, 2022.
62 T. Williams, C. Kelley and C. Bersch, *et al. Gnuplot 5.0: An Interactive Plotting Program*, 2017.